Ion uptake pathways in European sea bass Dicentrarchus labrax

Eva Blondeau-Bidet, Junya Hiroi, Catherine Lorin-Nebel

Ion uptake pathways in European sea bass *Dicentrarchus labrax*

Eva Blondeau-Bidet[1], Junya Hiroi[2], Catherine Lorin-Nebel[1]*

[1]Université Montpellier, UMR 9190 MARBEC, UM-CNRS-IRD-IFREMER, cc 092, Place E. Bataillon, 34095 Montpellier, cedex05, France

[2]Department of Anatomy, St. Marianna University School of Medicine, 2-16-1 Sugao, Miyamae-ku, Kawasaki, 216-8511, Japan

*Corresponding author:
E-mail: Catherine.lorin@umontpellier.fr
Phone: +33 (0)4 67 14 9391
Fax: +33 (0)4 67 14 9390

Keywords

Teleost, Osmoregulation, Ion transporters, Na^+ uptake, NHE3, NCC2

1. Introduction

The gill is a key organ involved in Na^+ and Cl^- absorption in freshwater-acclimated fish contributing to the maintenance of body fluid ionic homeostasis. As multifunctional organ, the fish gill is also a crucial organ responsible for acid-base balance and nitrogen excretion (Dymowska et al., 2012; Hwang et al., 2011; Hwang and Lin, 2013). Among teleost species, a diversity of ionocyte subtypes have been identified in fresh water (FW) notably in zebrafish *Danio rerio*, rainbow trout *Oncorhynchus mykiss*, medaka *Oryzias latipes* and Mozambique tilapia *Oreochromis mossambicus* (Dymowska et al., 2012; Hsu et al., 2014; Hwang, 2009). Apical Na^+ uptake mechanisms have been thoroughly discussed in teleosts in the last decade and implicate Na^+/H^+-exchangers (NHEs), Na^+ channels (acid-sensing ion channels, ASICs) energized by an electrical gradient generated by apical V-type H^+ ATPase (VHA) and/or Na^+/Cl^- cotransporters (fish-specific NCC2/NCC-like (*slc12a10*)) coupled to basolateral NKA and chloride channels (Hwang et al., 2011; Kumai and Perry, 2012). Na^+/H^+ exchangers (SLC9A family) are considered as main actors in apical Na^+ uptake, acid excretion, and can be functionally coupled to ammonia excretion in fish gill ionocytes. In freshwater-type ionocyte models of several species, NHE2 and/or NHE3 have been shown to localize in apical membranes to lead to an acid-trapping mechanism facilitating NH_4^+ excretion via basolateral RHBG and apical RHCG1. Extracellular NH_3 then combines with H^+ to form NH_4^+ covering the gill boundary layer, which leads to an increase in pH and favors the functioning of NHE (2/3) to take up Na^+ in exchange for H^+ (Cooper et al., 2013; Shih et al., 2012; Weihrauch et al., 2009). In the zebrafish cell model (HR cell), NHE3b, VHA and RHCG1 seem to colocalize in apical membranes and basolateral Na^+/K^+-ATPase is weakly expressed (Shih et al., 2008; Yan et al., 2007). NHE (2/3) has also been identified in PNA+ ionocytes of rainbow trout (for a review, see Dymowska et al., 2012). NHE2a has been shown in cuboidal cells of killifish *Fundulus heteroclitus*, the cell type responsible for Na^+ uptake (Edwards et al., 2010; Laurent et al., 2006). As VHA is expressed in basolateral membranes of

killifish cuboidal cells, Na^+ uptake seems not to be coupled to active proton excretion in this species (Katoh et al., 2003). There is also evidence that NHE2 and NHE3 are expressed in gill ionocytes of teleosts maintained in seawater (SW), playing critical roles in acid secretion (Chen et al., 2017; Claiborne et al., 1999; Liu et al., 2016; Weihrauch et al., 2009). In many teleost species, *nhe3* mRNA expression is high in FW compared to SW (Bollinger et al., 2016; Hiroi et al., 2008; Inokuchi et al., 2008; Watanabe et al., 2008) except in the climbing perch *Anabas testudineus,* where the opposite pattern has been shown with increased *nhe3* mRNA and NHE3 protein expression in SW (Chen et al., 2017). In this latter species, NKA α1c-immunoreactive ionocytes express NHE3 and RHCG2 in basolateral membranes and lack apical RHCG1, the exact function of these cells remains to be determined. Several paralogs have been identified in teleosts for *nhe* (1, 2, 3) probably due to putative genome duplication events (Glasauer and Neuhauss, 2014; Meyer and Van de Peer, 2005). Two or three *nhe2* paralogous genes have been identified in *F. heteroclitus*, *Takifugu rubripes*, *Gasterosteus aculeatus,* and the longhorn sculpin *Myoxocephalus octodecemspinosus* but functional differences remain to be analyzed (Edwards et al., 2010). Contrary to NHE2 and 3, NHE1 has been shown to be expressed in basolateral membranes and is mainly involved in pH homeostasis and cell volume regulation of epithelial and non-epithelial cells (Tse et al., 1993). Its expression increases following exposure to environmental hypercapnia in SW of several species and has been considered as protein involved in H^+ excretion to compensate for intracellular acidosis (Edwards et al., 2005).

Another Na^+ uptake model involves an apical Na^+ channel electrochemically coupled to the apical VHA. As epithelial Na^+ channels (ENaC) present in mammals are not present in teleost genomes, including the European sea bass, another Na^+ channel might be present in apical membranes of ionocytes to take up Na^+ in Na^+-poor environments. The presence of apical ASIC4 (acid-sensing ion channel 4) has been shown in gill ionocytes of two teleost species, the rainbow trout (in PNA+ ionocytes) (Dymowska et al., 2014) and zebrafish (in HR cells) (Dymowska et al., 2015). Zebrafish HR cells express NHE3b in apical membranes suggesting colocalization of VHA, NHE3b and ASIC4 in this cell type (Guh and Hwang, 2017). ASIC4 could thus, beside NHE3b, be part of a secondary Na^+ uptake mechanism in these cells.

Coupled Na^+/Cl^- uptake has been suggested to occur through Na^+/Cl^- cotransporters from the SLC12 family. Na^+/Cl^- cotransporters are called *ncc1 (slc12a3)* or *ncc2 (or ncc-like) (slc12a10).* The latter have been analyzed in different teleost species (Breves et al., 2014; Hiroi et al., 2008; Hsu et al., 2014; Inokuchi et al., 2017; Takei et al., 2014; Wang et al., 2009). Among different paralogs belonging to the *ncc2* family, zebrafish *slc12a10.2* was specifically expressed in the gills and its expression is stimulated in a low-Cl^- environment and not in a low-Na^+ environment (Wang et al., 2009). Hwang's group also showed that *slc12a10.1* seems to be predominantly expressed in the kidney and not in the gills of this species. In Mozambique tilapia *O. mossambicus* however, branchial *ncc2 (slc12a10)* was highly expressed in FW compared to SW (Inokuchi et al., 2008). In another tilapia species, *Oreochromis niloticus, ncc2 (slc12a10.2)* has been shown to be activated by prolactin (Breves et al., 2014).

In the European sea bass *Dicentrarchus labrax*, Na^+ uptake mechanisms as well as ionocyte subtypes have not been clearly identified in FW. Sea bass are euryhaline species that undertake seasonal migrations to low-salinity habitats like estuaries and lagoons and thus have to be able to rapidly activate efficient ion uptake and/or ion secretion mechanisms according to salinity. Several studies have shown that sea bass are able to tolerate FW for several weeks (Bodinier et al., 2009; Bossus et al., 2013 ; Lorin-Nebel et al., 2006). In late juveniles maintained in FW for two weeks, plasma Na^+, contrary to plasma Cl^-, was maintained constant without a significant decrease, suggesting efficient Na^+ uptake and reabsorption at the gill and kidney levels (Masroor et al., 2018). There is evidence of increased branchial *nka α1a (atp1a1a)* expression (Blondeau-Bidet et al., 2016), the predominant NKA α1 isoform in sea bass gills, contributing to increased NKA activity in FW (Masroor et al., 2018; Nebel et al., 2005). To our knowledge, no data are available on the presence and induction of diverse ion transporters favoring Na^+ uptake in sea bass gills in FW. This raises the question if sea bass gills present an ionocyte subtype that would be involved in proton-facilitated ammonia excretion and Na^+ uptake as shown in other species that experience low-salinity environments during their life cycle.

99 The objectives of the present study are to i) characterize main Na^+/H^+-exchangers (NHEs) in sea bass
100 osmoregulatory organs ; ii) identify transporters potentially involved in branchial Na^+ uptake and iii)
101 identify a new ionocyte subtype in European sea bass gills, the NHE3-type ionocyte.

102

103 ## 2. Material and Methods

104 ### 2.1. Experimental conditions

105 European sea bass *Dicentrarchus labrax* were obtained from the Ifremer Station at Palavas-les-Flots
106 (Hérault, France). Two batches of fish were used in these experiments. For quantitative real-time PCR
107 and immunocytochemistry (batch 1), the sampled fish average fork length was 20.77±1.32 cm (mean ±
108 SD) and average weight was 86.87±20.23 g. For identification of paralogous genes in the main
109 osmoregulatory tissues (gills, kidney and posterior intestine) (batch 2), the sampled fish average fork
110 length was 12.32±1.70 cm (mean ± SD) and weight was 21.62±9.92 g.

111 Fish were brought to the Montpellier University and maintained for one week in 3,500 L tanks
112 containing natural seawater (SW) from the Mediterranean sea at 38 ‰ and 18 °C, pH=7.78 under a 12
113 h light/12 h dark photoperiod. Fish were then transferred to smaller 200 L tanks either containing
114 dechlorinated tap water (FW) or SW and were maintained in this salinity until sampling. Fish were
115 respectively maintained in SW and FW for 2 weeks (medium term, batch 1) or 4 months (long term,
116 batch 2) before sampling. Ionic composition (in $mEq.L^{-1}$) of the FW was Na^+ (0.12), K^+ (0.04), Ca^{2+}
117 (5.70), Mg^{2+} (0.29), Cl^- (0.98), NO_3^- (0.06) and SO_4^{2-} (0.61) and pH=8.58. Water was aerated and
118 mechanically/biologically filtered (Eheim System, Lens, Pas-de-Calais, France). Temperature, salinity,
119 oxygen and nitrogen levels were checked regularly. 10 % of the water in each tank was changed
120 regularly using a siphon tube. The tank was then immediately refilled with water at the same salinity
121 (either SW or dechlorinated FW) and temperature. Fish were fed with fish granules (Aphymar feed,
122 Mèze, Hérault, France) until 2 days before sampling. At the end of the experiment, fish were
123 anesthetized in a solution of phenoxy-2-ethanol (0.24 $ml.L^{-1}$) (batch 1) or benzocaine (1 $ml.L^{-1}$) (batch
124 2) prior to any manipulation. The experiments were conducted according to the guidelines of the

European Union (directive 86/609) and of the French law (decree 87/848) regulating animal experimentation.

2.2 Phylogenetic analysis and protein structure

Phylogenetic analyses of *nhe2 (slc9a2)* (Fig. 1), *ncc (slc12a3)* (Fig. 2) and *nhe3 (slc9a3)* (Fig. 1S) have been performed. Nucleotide sequences of different teleosts and mammalians were obtained at Ensembl or NCBI (Table 1, 2, 1S). Sea bass sequences were obtained from the sea bass genome project (Tine et al., 2014). Multiple nucleotide alignments were performed with MUSCLE V3.8.31 (Edgar, 2004) and ambiguous regions were removed with Gblocks V0.91b (Talavera and Castresana, 2007). Best model of evolution was selected using Modelgenerator V.85 (Keane et al., 2006) following the corrected Akaike Information Criterion (with four discrete gamma categories) and used to construct phylogenetic trees. Phylogenetic trees were inferred using the maximum likelihood method implemented in the PhyML program (v3.1/3.0 aLRT) (Guindon and Gascuel, 2003) with the General Time Reversible (GTR) model of substitution (Tavaré, 1986) with discrete-gamma distributed rate variation and with the transversional model (TVM) (Posada 2003) with discrete-gamma distributed rate variation and estimated proportion of invariable sites, combined to the best "Nearest Neighbor Interchange" (NNI). The trees were generated and robustness of the phylogeny assumption was evaluated by the approximate likelihood test (aLRT) SH-like branch support and by bootstrapping procedure from 1000 data set replicates. As outgroup species, we used sequences of chicken (*Gallus gallus*), rabbit (*Oryctolagus cuniculus*) and human (*Homo sapiens*) for phylogenetic analyses on *nhe3*. Multiple protein sequence alignment and amino acid identities (in %) were performed with MUSCLE V3.8.31 (Edgar, 2004) implemented in Geneious® 9.1.8 software (Biomatters). The prediction of membrane topology was performed with PolyPhobius (Käll et al., 2005). The prediction of potential N-glycosylation was done using ScanProsite (http://www.expasy.ch/tools/scanprosite/).

151 **2.3 RNA extraction and complementary DNA (cDNA) synthesis**

152 Total RNA was extracted from gills, kidney and posterior intestine using Trizol ® reagent and
153 processed according to the manufacturer's instructions. RNA quantity was assessed by measuring the
154 A260/A280 ratio using the NanoDrop® ND-1000 V3300 Spectrophotometer (Nanodrop Technology
155 Inc., Wilmongton, DE, USA) and RNA integrity was checked using an Agilent Bioanalyzer 2100
156 equipped with an RNA Nano Chip (Agilent Technologies, CA, USA). RNA Integrity Numbers (RIN)
157 were greater than 7. One microgram of total RNA was treated with DNase I amplification grade
158 (Invitrogen™, Life Technologies) and the first strand of complementary DNA (cDNA) was generated
159 using Random Primers oligonucleotides (Invitrogen™) and the M-MLV reverse transcriptase
160 (Invitrogen™), following the manufacturer's guidelines. PCR products were sequenced by Sanger
161 sequencing in order to validate the identity of the amplified sequences in comparison with the sea bass
162 genome.

163 **2.4 Tissue distribution analysis using RT-PCR**

164 Tissue distribution of *nhe1 (slc9a1), nhe1β-like (slc9a1β-like), nhe2a (slc9a2.1)*, *nhe2b (slc9a2.2),*
165 *nhe2c (slc9a2.3)* and *nhe3* (*scl9a3*) were examined in gills (first right gill arch), posterior intestine and
166 posterior kidney of sea bass. cDNA of 4 animals per salinity (SW and FW) were pooled in equal
167 amounts. For PCR amplification, 1µL of diluted cDNA (at 1/10 for *nhe1 (slc9a1) , nhe1β-like*
168 *(slc9a1β-like), nhe2a (slc9a2.1), nhe2b (slc9a2.2), nhe2c (slc9a2.3)* and at 1/20 for *nhe3 (slc9a3*) was
169 used as template in a final reaction volume of 25 µL containing 5 µL (1X) of 5X Green GoTaq® Flexi
170 Buffer, 0.5 µL (0.2 mM) of dNTP mix (10 mM each), 0.13 µL (1.25 units) of GoTaq® G2 Flexi DNA
171 Polymerase (Promega, Madison, USA), 2 µL (2 mM) of $MgCl_2$ 0.5 µL (0.2 µM) of each primer (Table
172 3) and 15.87 µL of nuclease-free water. Conditions used in the PCR were as follows : 2 min
173 denaturation at 95 °C followed by 35 cycles (95 °C for 30 s, 61 °C for 45 s and 72 °C for 1 min)
174 followed by a final elongation step at 72 °C for 4 min. The resulting PCR products were visualized by
175 electrophoresis on a 2 % agarose gel containing 0.5 µg/mL GelRed ® (Biotium, USA) and viewed
176 under UV light on a Gel Doc 1000 system (Bio-Rad, UK).

177 **2.5 Quantitative real-time RT-PCR (qRT-PCR)**

178 Eight fish per salinity treatment were analyzed for gene expression studies. An Echo®525 liquid
179 handling system (Labcyte Inc., San Jose, CA, USA) was used to dispense 0.75 µL of LightCycler-
180 FastStart DNA Master SYBR-Green I™ Mix (Roche, Mannheim, Germany), 0.037 µL of each primer
181 (at 0.5 µM), 0.21 µL of ultra-pure water and 0.5 µL of diluted cDNA into a 384-well reaction plate.
182 Each sample was run in triplicate. The qRT-PCR conditions were as follows: denaturation at 95 °C for
183 10 min, followed by 45 cycles of amplification (95 °C, 15 s), hybridization (60 °C, 5 s) and elongation
184 (72 °C, 10 s), and a final step at 40 °C for 30 s. A melting curve program was performed to control the
185 amplification specificity. Ultra-pure water was used as a no-template control in the qRT-PCR.
186 Efficiencies were between 1.9 and 2.1 according to the considered primer pair.

187 The expression level was normalized using the expression of the elongation factor *ef1α* and ubiquitin
188 like and ribosomal protein S30 fusion gene (*fau*). *ef1α* has been already successfully used in this
189 species (Blondeau-Bidet et al., 2016) and *fau* was recommended for sea bass qRT-PCR normalization
190 by Mitter et al. (2009). Relative expression levels were calculated using the comparative Ct method
191 (threshold cycle number) by averaging the results normalized against both *fau* and *ef1α* (Pfaffl 2001).
192 Ct of both reference genes did not vary according to salinity conditions.

193 **2.6 Immunocytochemistry**

194 The first left gill arch of three animals per condition was fixed for 48 h by immersion in Bouin's
195 fixative. After rinsing in 70 % ethanol, samples were dehydrated in a graded ethanol series and
196 embedded in Paraplast (Sigma). Transverse sections (4 µm) were cut on a Leitz Wetzlar microtome,
197 collected on poly-L-lysine-coated glass slides and stored at room temperature until the
198 immunostaining procedure. For co-immunolabelling, sections were dewaxed (LMR and butanol),
199 hydrated through a descending series of ethanol baths (from 100 % to 50 %) and rinsed in phosphate-
200 buffered saline (PBS; 137 mM NaCl, 2.7 mM KCl, 10 mM phosphate buffer, pH 7.4, Sigma). Slides
201 were then immersed in a sodium citrate buffer (Tri-sodium citrate dihydrate in 0.05 % Tween 20, pH
202 6) and placed in a microwave oven (at 80 % power 2 times 1 min) to reveal antigenic sites. The slides

were then incubated for 10 min in 0.02 % Tween 20 in PBS supplemented with NaCl to 286.5 mM, pH 7.3. After saturation in 5 % bovine serum albumin (BSA) in PBS at room temperature for 20 min, the slides were rinsed twice with PBS. Primary labelling was performed overnight at 4 °C (NHE3) followed by three washes in PBS, then 2h at room temperature (NKA and T4) in a wet chamber. The following primary antibodies diluted in 0.5 % BSA-PBS were used : mouse monoclonal antibody (α5) anti-Na^+/K^+-ATPase deposited to the DSHB by Fambrough, D.M. (DSHB Hybridoma Product α5) (Hybridoma Bank, University of Iowa) at 10 µg.mL^{-1}, mouse T4 (SLC12A1/A2) antibody deposited to the DSHB by Lytle, C. / Forbush III, B. (DSHB Hybridoma Product T4) at 7 µg.mL^{-1} and rabbit polyclonal antibody raised against rainbow trout (*O. mykiss*) Na^+/H^+-exchanger 3b (NHE3b) at 20 µg.mL^{-1}. NHE3 antibody was raised against a cocktail of two peptides from rainbow trout NHE3b. The sequences of these peptides are 100 % identical to sea-bass NHE3 (SLC9A3). NHE3 antibody was already used successfully in other teleost species (Christensen et al., 2012; Seo et al., 2013; Wright et al., 2016). Negative control slides without the primary antibody were also prepared. After three washes in PBS to remove unbound antibody, the sections were incubated for 1 h with the secondary antibodies at room temperature (anti-mouse Alexa Fluor®488 at 10 µg.mL^{-1} and anti-rabbit Rhodamine at 4 µg.mL^{-1}). Following 3 washes, nuclei were counterstained with 4',6-diamidino-2-phenylindole (DAPI) during 2 min, then washed 3 times and sections were mounted in an anti-bleaching mounting medium (Immunohistomount, Santa Cruz Biotechnology). Observations were done with a Leica TCS SP2 confocal microscope of the MRI platform, at Montpellier University.

2.7 Statistical analysis

Statistical analyses were performed using Graphpad Prism (version 6, GraphPad Software Incorporated, La Jolla, CA 268, USA). Due to the small sample size (N=8), a non-parametric Mann-Whitney U-test and a Kruskal-Wallis test were used for statistical comparisons. To determine differences between conditions, a post-hoc test was performed. Data are presented as means ± SEM unless noted otherwise, and the level of statistical significance was set at $p < 0.05$

3. Results

3.1 Identification of sea bass *nhe* paralogous genes and phylogeny

In the sea bass genome, we found several paralogous genes for Na^+/H^+-exchangers (*slc9a)* among them two *nhe1* (*slc9a1)* (annotated *slc9a1* and *slc9a1β-like*), three *nhe2* (*slc9a2)* that we will call in this study (*nhe2a (slc9a2.1), nhe2b (slc9a2.2)* and *nhe2c* (*slc9a2.3*) according to their phylogenetic position (Fig. 1) and only one *nhe3* (*slc9a3)* (Fig. 1S). Sea bass NHE3 is highly homologous to other NHE3 of the longhorn sculpin *M. octodecemspinosus*, the stickleback *G. aculeatus,* and the climbing perch (*A. testudineus*) (81 %, 78 %and 76 % respectively).

Maximum likelihood analysis generated a tree of the three *D. labrax nhe2* subtypes against sequences of selected acanthomorph and salmonid species. Analysis of teleost genomes revealed the presence of one, two (*nhe2a* and *b* in *F. heteroclitus and T. rubripes, nhe2b and nhe2c in M. octodecemspinosus*) or three (*nhe2a*, *b* and *c* in *G. aculeatus*) *nhe2* subtypes (Edwards et al., 2010). *D. labrax nhe2a, nhe2b and nhe2c* group with other *nhe2a, nhe2b* and *nhe2c* sequences (Fig. 1). The human (*H. sapiens*), chicken (*G. gallus*) and rabbit (*O. cuniculus*) branched at the basis of the teleost *slc9a2* paralog clade with respect to their phylogenetic position. NHE2b and NHE2c amino acid sequences of *D. labrax* exhibited a percentage identity of 79 %, whereas NHE2a showed a lower percentage identity with NHE2b and NHE2c (48 % and 46 %, respectively).

3.2 Characterization of sea bass *ncc1/ncc2* paralogous genes and phylogeny

Three *ncc1/ncc2* genes have been identified in the sea bass genome called *slc12a3*, *slc12a3-like* and *slc12a10*.2. *Slc12a3* (*ncc1*, 3081 bp) could not be detected in sea bass gills in this study (not shown). A sequence of 486 bp was identified for *slc12a10.2 (ncc2b)*, that is phylogenetically very close to *slc12a3-like* (2802 bp) and other teleost *slc12a10 (ncc2)* sequences (Fig. 2). We thus propose that sea bass *slc12a3-like* can be considered as *ncc2* compared to our phylogenetic tree conducted on *slc12a10/slc12a3* sequences (Takei et al., 2014; Wang et al., 2009). The tree shows two clades, the *slc12a3/ncc1* clade and the fish-specific *slc12a10/ncc2* clade. All teleost species examined have only

254 one *slc12a3/ncc1* gene, grouped in the same clade (blue frame, Fig. 2). The s*lc12a10* and *slc12a3-like*
255 sequences of sea bass were very close and belonged to the *ncc2* clade (green frame in Fig. 2).

256 The identity of the sea bass NCC1 and NCC2 (a, b) amino acid sequences were confirmed by
257 comparison with sequences of teleost species. Interestingly, sea bass NCC1 showed a low percentage
258 identity with sea bass NCC2a and NCC2b (48 % and 30 %, respectively). Sea bass NCC1 was highly
259 homologous to NCC1 of killifish *F. heteroclitus* and stickleback *G. aculeatus* (81 % and 79 %
260 respectively). Sea bass NCC2 a and b showed an amino acid sequence identity of 72 % and 82 %,
261 respectively, with the killifish ortholog, NCC2.

262 Prediction of the transmembrane topology revealed the existence of 12 potential transmembrane-
263 spanning segments (Fig. S2) as previously reported in zebrafish and winter flounder
264 (*Pseudopleuronectes americanus*) NCCs (Wang et al., 2009 and Gamba et al. 1993). The search for
265 potential N-glycosylation sites showed 2 highly conserved sites (Asn 364 and Asn 551) among all the
266 analysed NCCs (see yellow highlighting, Fig. S2). The N-glycosylation site at position 411 in fish
267 NCC1 and mammalian NCC seems to be absent in fish NCC2 sequences. In fish NCC2, two other N-
268 glycosylation sites are present (Asn 409 and Asn 418) close to this region. At position 433, the N-
269 glycosylation site was only conserved in mammalian NCC and teleost NCC2 sequences whereas Asn
270 789 was conserved in mammal NCC only. We have identified several amino acids conserved only
271 among mammal NCC and fish NCC1 sequences (Fig. S2, red boxes). Several amino acids are
272 conserved only among the teleost NCC1 and NCC2 sequences (Fig. S2, blue boxes). We also
273 identified conserved amino acids between mammal and fish NCC2 sequences (Fig S2, green boxes).

274

275 **3.3 mRNA expression patterns of *nhe* paralogs in osmoregulatory tissues**

276 Tissue distribution of *nhe* paralogs were compared in gills, posterior kidney and posterior
277 intestine/rectum in SW and FW after 4 months of salinity acclimation with *fau* as the internal control
278 (Fig. 3). *Nhe1* (*slc9a1*) was expressed in the all osmoregulatory tissues analysed, notably in the
279 posterior intestine/rectum and FW kidney. *Nhe1β-like* (*slc9a1β-like*) was expressed in gills and kidney

in SW and FW. *Nhe2b* (*slc9a2.2*) and *nhe2c* (*slc9a2.3*) were specifically expressed in the gill tissue and present at both salinities. *Nhe3* (*slc9a3)* was highly expressed in the gills and posterior kidney at both salinities.

3.4 Gene expression

Nhe paralogous genes were quantified in SW and FW (Fig. 4A). Among them, *nhe2a (slc9a2.1)* showed a nearly not detectable band (Fig. 3) and has therefore not been quantified in sea bass gills. Significant expression differences between salinities were observed for *nhe1β-like* (*slc9a1β-like),* *nhe2c* (*slc9a2.3)* and *nhe3* (*slc9a3)* transcripts (Fig. 4A). *Nhe1β-like (slc9a1β-like*) and *nhe2c* (*slc9a2.3)* expression were significantly higher in SW than in FW, respectively by 1.7-fold ($p < 0.01$) and by 28-fold ($p < 0.001$). Conversely, mRNA levels of *nhe3* (*slc9a3)* were significantly higher in FW than in SW, by 2.8-fold ($p < 0.01$). The expression of *nhe3* (*slc9a3)* was high compared to *nhe2c* (*slc9a2.3)* mRNA levels, by 17-fold in SW ($p = 0.024$) and by 1351-fold in FW ($p < 0.0001$).

The relative expression of *nkcc1* (*slc12a2)* and *ncc2a* (*slc12a3-like)* (Fig. 4B) were examined in SW and FW. mRNA levels of *nkcc1* (*slc12a2)* was significantly higher in SW than in FW, by 1.7-fold ($p = 0.001$). The expression of *ncc2a* (*slc12a3-like)* showed the opposite trend, with a 3-fold overexpression in FW compared to SW ($p = 0.0003$).

In the sea bass genome, two *rhcg* sequences have been identified, named *rhcg1* and *rhcg*. We renamed *rhcg* to *rhcg2* according to its phylogenetic position (not shown). Among the 17 different carbonic anhydrase genes detected in the sea bass genome, we quantified the *cahz* gene that grouped with the teleost CA2-like-a clade, as defined by Lin et al. (2008) including medaka CA2-like a and trout cytoplasmic CAc (Esbaugh et al., 2005; Gilmour, 2012). CAC amino-acid sequence of *D. labrax* exhibited a percentage identity of 84 % and 81 % respectively with CA2-like a of *O. latipes* and CAc of *O. mykiss*, respectively. The CAC sequence of *D. labrax* showed a lower homology with CA2-like b of *O. latipes* and CAb of *O. mykiss* (70 % and 78 %, respectively). We considered this gene as the cytoplasmic carbonic anhydrase, and therefore we called it *cac* in this paper.

Relative expression of branchial *vha-a (atp6v1a), vha-b (atp6v1b2), nka α1a (atp1a1a), nka α1b (atp1a1b)*, cytoplasmic carbonic anhydrase *cac*, sodium bicarbonate cotransporter *nbc1 (slc4a4),* ammonia transporters (*rhbg, rhcg1* and *rhcg2*) are shown in Fig. 4C. Acid-sensing ion channel 4 gene (*asic4*) has also been tested as a potential Na^+ uptake channel, but results fell outside the range of quantifiable values (Ct>31) and could not be interpreted. FW challenge induced *nka α1a* (*atp1a1a)* expression by 2-fold ($p = 0.0006$) as well as the presumably apical ammonia transporter *rhcg1*, by 4-fold ($p = 0.0001$). Expression of both *vha* subunit-*a* and *b* (atp6v1) were low and did not change according to salinity. *Rhcg2* was well expressed at both salinities and *cac* showed a slightly but not significantly higher expression in FW ($p = 0.06$). Transcript levels of reference genes *ef1α* and *fau* did not change between salinities ($p > 0.57$ and $p > 0.87$, respectively).

3.5 Immunolocalization

Na^+/K^+-ATPase was coimmunostained with NHE3 to identify NHE3-immunopositive ionocytes in FW (Fig. 5). NHE3 was localized in apical membranes of ionocytes expressing NKA (Fig. 5A, B1, B2). NHE3-expressing cells were generally localized on lamella and showed a large apical surface (Fig. 5A). Few NHE3-immunopositive cells have been detected on filaments. Higher magnification images (Fig. 5B1, B2) showed that apical NHE3 is in contact with the surrounding water whereas basolateral surfaces of NHE3-expressing cells are in contact with blood.

We also used NHE3/T4 (NKCC1,2/NCC) coimmunostaining in SW (Fig. 6A1, A2) and FW gills (Fig. 6B1, B2, C1, C2). In SW, T4 immunostaining was detected in all ionocytes that are located on filaments and showed a strong basolateral staining (Fig. 6A1). NHE3 could not be detected at this salinity (Fig. 6A2). In FW, NHE3-immunopositive cells were also immunopositive for T4, but on basolateral membranes (Fig. 6B1, B2, C1, C2). Most ionocytes present on filaments showed a low basolateral T4 staining and no apical NHE3 (Fig. 6C2, arrow).

NKA/T4 (NKCC1,2/NCC) coimmunostained gills from freshwater-exposed sea bass showed intracellular colocalization of basolateral NKCC1 (T4) and NKA in some lamellar cells indicated in Fig. 7 (indicated by '*'). These cells did not exhibit apical T4 immunolabeling. Another ionocyte subtypes was localized on the filament and at the base of the lamella with an apical T4

immunostaining, presumably NCC2. NCC2 cells, contrary to the previous described ionocyte subtype, did no show strong basolateral T4 (NKCC1). Two image from a z-stack were shown (Fig. 7A1, A2) showing several ionocytes with faint apical T4 staining identified by a number. Cells without number did not show clear apical T4 throughout the z-stack.

4. Discussion

In the last decade, different sodium uptake pathways have been investigated in several teleost species (zebrafish, medaka, trout and tilapia notably) (Dymowska et al., 2012; Hwang, 2011) but it is important to complete ion uptake models in other ecologically relevant euryhaline species that encounter strong salinity fluctuations in their natural habitat as the European sea bass. The sea bass is an important species for aquaculture and fisheries and its genome has been fully sequenced, assembled and annotated (Tine et al., 2014). The sea bass is therefore an excellent model for analyzing osmoregulatory mechanisms at different salinities.

It is now admitted that Na^+ uptake is strongly linked to acid-base regulation and nitrogen excretion in specific ionocyte subtypes (Weihrauch et al., 2009; Wright and Wood, 2009). Na^+ uptake can also be coupled to Cl^- uptake in species that express Na^+/Cl^- cotransporters from the NCC2 (SLC12A10) clades (Hiroi and McCormick, 2012; Hsu et al., 2014) or mediated by a Na^+ channel coupled to apical VHA (Dymowska et al., 2012). The predominance of one mechanism of ion uptake over the other is highly dependent on the environmental stimuli (ion strength, salinity, pH) and the considered species. Unlike zebrafish and trout, sea bass *asic4* seems not to be expressed in FW gills. Other ASICs should be analyzed in future to explore if other members of the ENaC/DEG (degenerin) family might be involved in Na^+ uptake in sea bass gills.

4.1 NHE3 as a key protein in gills of sea bass maintained in fresh water

We have shown for the first time in European sea bass that branchial *nhe3* is significantly more expressed following a FW transfer and its expression is much higher than all other *nhe* paralogous genes analyzed in this study, clearly showing its major role in sea bass gills, notably in FW. It has to be noted that *nhe3* is also highly expressed in the posterior kidney and could thus also have a role in

renal Na^+ re-uptake and acid secretion. Only one NHE3 isoform is present in the sea bass genome and it is highly homologous to NHE3 of species showing only one NHE3 paralogous protein and potentially sharing a common NHE3 function. Immunolocalization of NHE3 shows an apical localization in a subset of ionocytes that also express Na^+/K^+-ATPase as previously shown in rainbow trout PNA+ MRC, zebrafish HR cells and Mozambique tilapia type-III ionocytes (Hiroi et al., 2008; Hwang, 2011; Inokuchi et al., 2008). We have not detected NHE3 in apical membranes of gill ionocytes from SW fish unlike previous data obtained in other species like Japanese sea bass (Inokuchi et al., 2017). NH_4^+-dependent Na^+ uptake has been identified in medaka, trout and zebrafish (Shih et al., 2012; Wright and Wood, 2009; Wu et al., 2010). In zebrafish HR cells, low-sodium water is a trigger for the differentiation of an apical protein complex involving NHE3b, RHCG1 and V-type H^+-ATPase (Shih et al., 2008). Our study shows that *vha* (*a* and *b* subunits) is not highly expressed and expression is not induced following FW challenge in sea bass gills. Sinha et al. (2015) however have shown that VHA activity is increased at low salinity (2.5 ‰) compared to SW. It is thus possible that posttranscriptional modifications activate VHA in sea bass FW gills. The involvement or not of VHA in the above-mentioned functional complex as well as its localization in ionocytes remain to be elucidated in sea bass.

Interestingly, expression of sea bass *rhcg1* and *nka α1a* increase significantly following FW challenge, however we do not know if RHCG1 is localized in NHE3-expressing cells as shown in other species (Nakada et al., 2007). Sea bass gill ionocyte density has previously been shown to increase significantly in FW compared to SW, notably due to an increase in lamellar ionocytes (Masroor et al., 2018). We have shown in this study that NHE3-immunopositive cells are essentially located on lamella. The slightly higher cytoplasmic carbonic anhydrase (*cac)* expression in FW gills could indicate an increased proton and bicarbonate supply for different transporters expressed in apical and basolateral membranes. Interestingly, NHE3-expressing cells also show basolateral T4 immunostaining which suggests the presence of NKCC1 in these cells as shown recently in the Japanese sea bass *Lateolabrax japonicus* (Inokuchi et al., 2017). In NHE3-expressing cells from the FW condition, T4 staining intensity is clearly lower than in ionocytes from fish maintained in SW condition. This may be linked to the lower branchial mRNA levels of *nkcc1 (slc12a2)* in FW

compared to SW. SW-type ionocytes may change their molecular setup and differentiate into FW-type cells expressing apical NHE3 and basal NKA and NKCC1. This hypothesis has been raised recently by Kaneko's group who reported in Japanese sea bass gills a transformation of SW-type cells to NHE3-type cells concomitant with a shift in their distribution from filaments to lamellae (Inokushi et al., 2017). In this earlier study, 10 days acclimated fish were used, similarly to our study were 2 weeks-transferred fish were analyzed. In Japanese sea bass, NHE3-NKCC1 expressing cells were called intermediate cells whereas a small percentage of NHE3 cells without basolateral NKCC1 were considered as fully FW-type cells. We have previously reported in European sea bass the presence of intermediate cells in FW lamella expressing basal NKCC1 using the T4 antibody in a time-series study following FW transfer (Lorin-Nebel et al., 2006). If European sea bass gills transform SW-type ionocytes into NHE3-NKCC1 cells upon FW transfer, this would certainly contribute to the high capacity of sea bass to maintain constant Na^+ levels in highly fluctuating salinities like Mediterranean lagoons.

Two *nhe2* paralogous genes are expressed in sea bass gills but their role in Na^+ uptake seems minor as they are not highly expressed in FW. Among the other *nhe* paralogs (besides *nhe3*) that have been analyzed in this study (*nhe1*, *nhe1β-like*, *nhe2a*, *nhe2b*, *nhe2c*), no induction has been detected in FW after the two-weeks salinity transfer. A time course sampling would be necessary to fully address the question on what *nhe* paralogs are induced following a FW challenge. The ubiquitous expression of *nhe1* in all analyzed tissues suggests a minor role in transepithelial ion uptake and rather a role in acid removal from the cytoplasm and cell volume regulation as reported previously. No *nhe1* expression difference between SW and FW has been shown in the rainbow trout in different tissues including gills, kidney and anterior intestine (Genz et al., 2011). Few studies have quantified the expression of different *nhe2* paralogs, notably *nhe2c* (Edwards et al., 2010). We have identified three *nhe2* paralogous genes with only two of them well expressed in the gills, *nhe2b* and *nhe2c*. No expression has been detected in the posterior kidney and posterior intestine/rectum. This is also the case in the toadfish *Opsanus tau*, where *nhe2* has not been detected in posterior intestine, neither in the rectum (Esbaugh and Grosell, 2014). It has to be noted that only one toadfish *nhe2* has been investigated, that seems to play an important role in the desalinization process in the oesophagus (Esbaugh and Grosell,

2014). *Nhe2b* and more strikingly *nhe2c* expressions are low in sea bass gills and the involvement of NHE2 in apical Na^+ uptake seems thus unlikely. In trout, high levels of apical NHE2 and NHE3 have been shown in PNA^+ MRC, a cell type rich in NKA, but lacking VHA (Ivanis et al., 2008). *Nhe2* sequence of trout is in the clade of sea bass *nhe2b*. Hypercapnia and increased cortisol levels seem to increase NHE2 levels in this species indicating a role in acid-base regulation (Ivanis et al., 2008). Despite its very low expression, sea bass *nhe2c* is about 28 times more expressed in SW than in FW suggesting its role in acid secretion as reported previously for several *nhe2/3* paralogs in SW (Chen et al., 2017; Claiborne et al., 1999; Liu et al., 2016). Contrary to trout *nhe2*, sea bass *nhe2b* and *nhe2c* are not expressed in the posterior kidney and intestine and *nhe2a* was not clearly detected in any osmoregulatory tissue. This is not the case in killifish, where NHE2a has been identified in cuboidal cells, the cell type expressing basolateral VHA and being involved in Na^+ uptake (Edwards et al., 2010; Laurent et al., 2006).

4.2 NCC2 in sea bass gills

We have shown here and in a previous study the presence of basolateral or apical T4 (NKCC1,2/NCC) immunostaining in gill ionocytes of sea bass transferred for two weeks to FW (Lorin-Nebel et al., 2006). In that earlier study, it has already been reported that following FW transfer, several ionocytes remain basolaterally immunostained. This could indicate the presence of NKCC1. Other ionocyte subtypes present an apical staining, presumably NCC2. In this study we showed that apical NCC2 staining was present in several ionocytes located essentially on the filament. Compared to our previous study (Lorin-Nebel et al., 2006), apical immunostaining was less intense, which is probably due to different conditions used for colocalization studies with NKA. A specific NCC1 or NCC2 antibody is necessary to identify the specific paralogous NCC protein. NKCC1/NCC immunopositive ionocytes have been identified with the T4 antibody that recognizes a large epitope (38kDa peptide fragment) partially common to several SLC12A isoforms including NKCC1, NKCC2, NCC1 and also NCC2. Apical staining using this antibody has further been shown in other teleost species in FW (Hiroi et al., 2008). In the sea bass genome, *slc12a3 (ncc1), slc12a3-like (ncc2a) and slc12a10 (ncc2b)* have been detected. *Slc12a3-like* was highly expressed in sea bass gills and was phylogenetically close to other

443 *ncc2* sequences. We therefore called it *ncc2a* and quantified its expression in our study. The small size
444 of the sequence of *slc12a10.2 (ncc2b)* (486 pb) and its close phylogenetic position to *slc12a3-like*
445 *(ncc2a)* suggests that these two genes may be splice variants or paralogs. *Ncc2a* was significantly
446 higher expressed in FW than in SW, whereas *nkcc1* (*slc12a2*) shows a decreased expression in FW
447 which suggests the differentiation of *ncc2a* expressing ionocytes in FW conditions.
448 We have shown for the first time in this study the presence of different ionocyte subtypes in sea bass
449 gills in FW with a NHE3-expressing ionocyte subtype, localized on lamella and potentially involved
450 in Na^+ uptake. This NKA-rich cell expresses apical Na^+/H^+-exchanger (NHE3, SLC9A3) and
451 basolateral T4, presumably NKCC1 (SLC12A2). This suggests a differentiation of a SW-type cell into
452 a FW-type cell as a response to salinity changes that often occur in natural habitats. The presence in
453 FW gills of ionocytes in the filament with high NKA immunostaining and apical T4 staining as well as
454 the high branchial expression of *ncc2a* suggest the presence of another cell type expressing apical
455 NCC2. It has not to be ruled out that other ionocyte subtypes exist in FW-acclimated sea bass as not
456 all NKA-positive ionocytes showed apical NHE3 or NCC2. These other ionocyte subtypes remain to
457 be characterized in European sea bass. The exact function of the two characterized ionocyte subtypes
458 and the proteins they express in sea bass exposed to various environments will be investigated further
459 in the future and will help to have a more comprehensive view on marine teleost salinity acclimation
460 strategies.
461

462 Acknowledgments
463 The authors would like to thank Thibaut L'Honoré for providing 4-months acclimated sea bass to
464 fresh water as well as Waliullah Masroor for providing some sea bass gill slides and Emilie Farcy for
465 providing *fau* primers. The authors also would like to thank Sophie Hermet for her help in the first
466 immunostaining tests, Philippe Clair from the qPCR CEMEB platform as well as the Montpellier
467 Ressources Imagerie (MRI) staff, Elodie Jublanc and Vicky Diakou, for their precious advice.

468

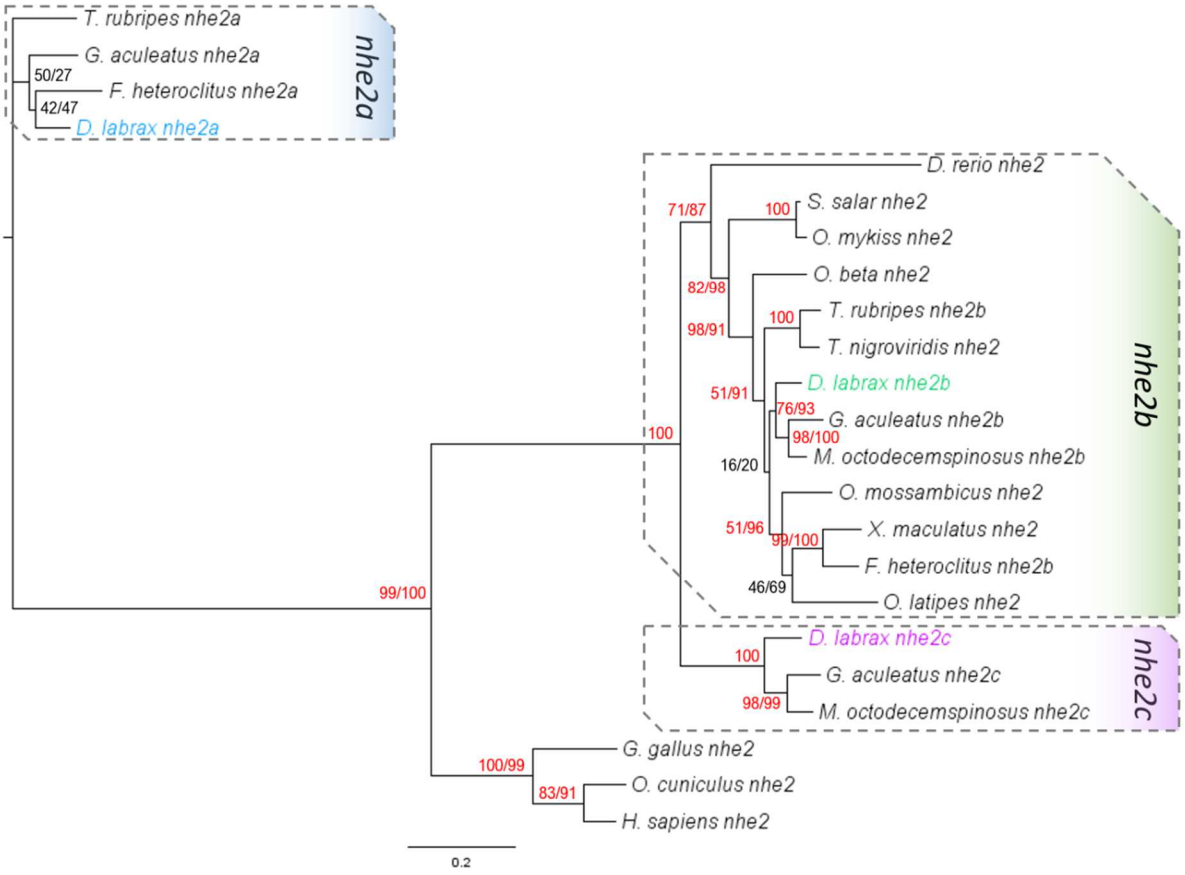

Fig. 1 Phylogenic tree of *nhe2* (*scl9a2)*. Phylogram of maximum likelihood relationships between *nhe2a, nhe2b* and *nhe2c* nucleotides sequences of representative acanthomorph and salmonid species. Branch lengths represent the degree of divergence, with the scale bar indicating the distance representing 0.2 substitutions per position. Bootstrap values (in %) and SH-like aLRT values are indicated for each node if different (in red color if confident). The blue frame mainly comprises sequences of teleost *nhe2a*. The green frame mainly comprises sequences of acantomorph *nhe2b* and salmonid *nhe2*. The purple frame mainly comprises sequences of teleost *nhe2c*.

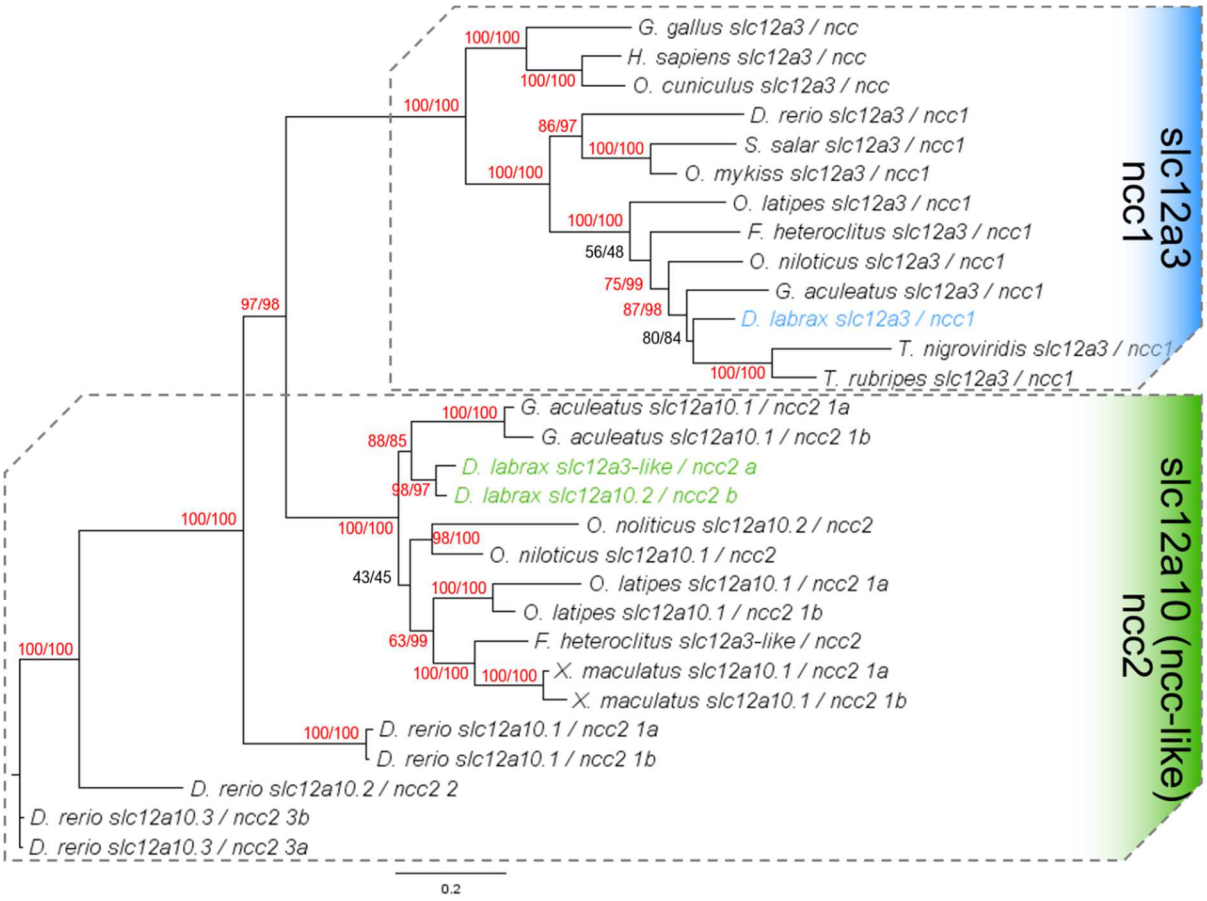

Fig. 2 Phylogenic tree of *ncc (slc12a3), ncc2a (slc12a3-like) and ncc2b (slc12a10.2)*. Phylogram of maximum likelihood relationships between *ncc1* and *ncc2* nucleotides sequences of representative acanthomorph and salmonid species. Branch lengths represent the degree of divergence, with the scale bar indicating the distance representing 0.2 substitutions per position. Bootstrap values (in %) and SH-like aLRT values are indicated for each node if different (in red color if confident). The blue frame mainly comprises sequences of teleost *ncc1*. The green frame mainly comprises sequences of acantomorph *ncc2*.

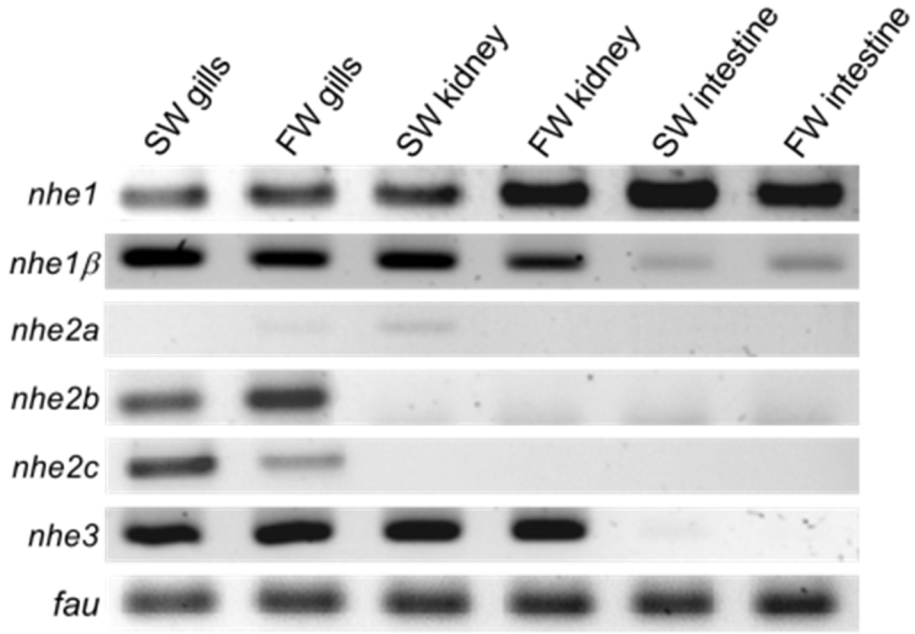

Fig. 3 Tissue distribution analysis of *nhe1 (slc9a1), nhe1β-like (slc9a1β -like)*, *nhe2a (slc9a2.1), nhe2b (slc9a2.2), nhe2c (slc9a2.3)* and *nhe3 (slc9a3)* in *D. labrax* acclimated to sea water or fresh water for 4 months. *fau* was used as the internal control.

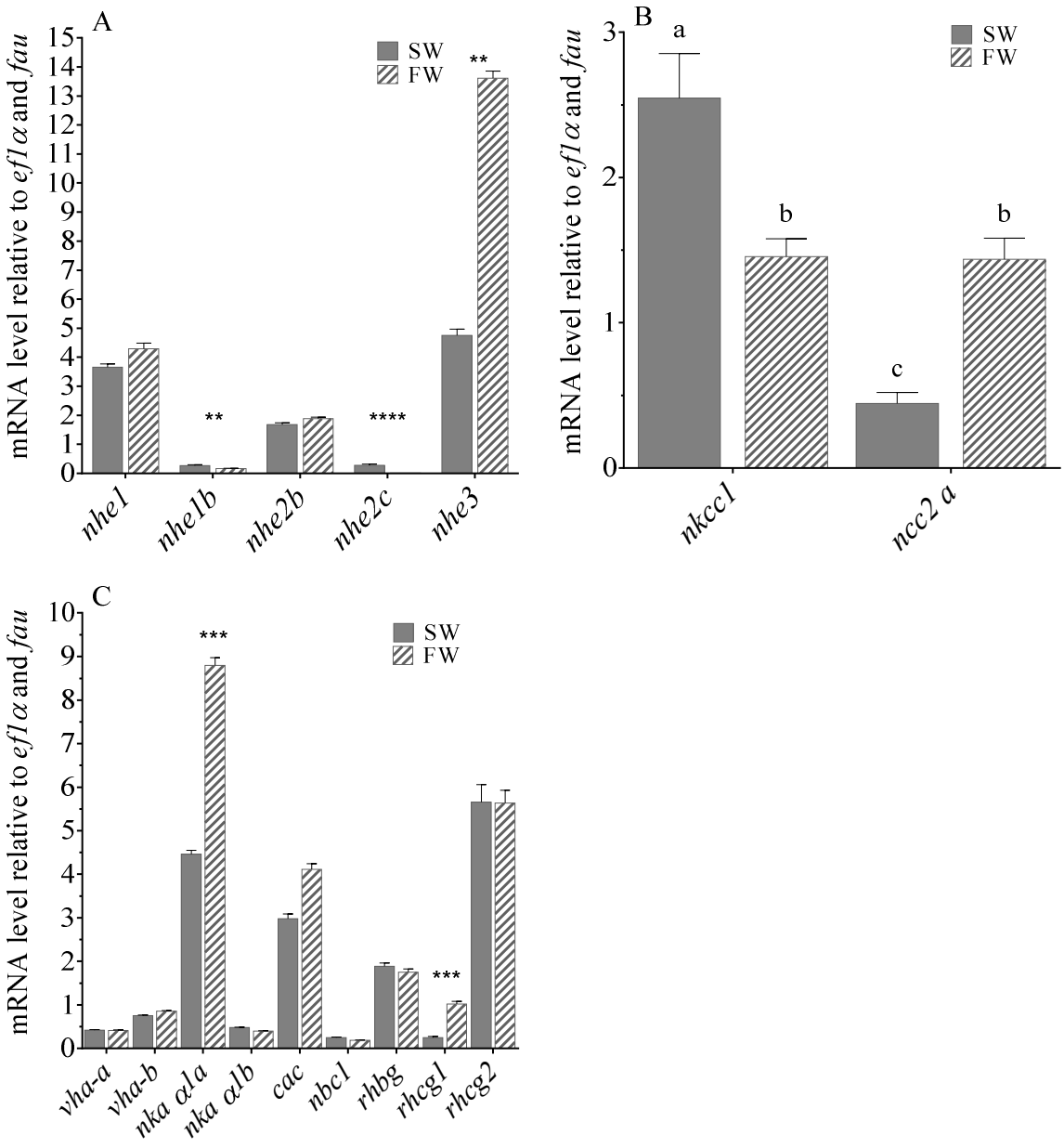

Fig. 4 Relative expression of (A) *nhe1 (slc9a1)*, *nhe1β-like (slc9a1-βlike)*, *nhe2b (slc9a2.2)*, *nhe2c (slc9a2.3)* and *nhe3 (slc9a3)*, (B) *nkcc1 (slc12a2)* and ncc2a (*slc12a3-like*) (C) *vha-a (atp6v1a)*, *vha-b (atp6v1b2)*, *nka α1a (atp1a1a)*, *nka α1b (atp1a1b)*, *cac,ncb1 (slc4a4) rhbg, rhcg1* and *rhcg2* in gills of *D. labrax* juveniles exposed to SW and FW for two weeks. The expression has been normalized according to the expression of the elongation factor *ef1α* and the ubiquitin like and ribosomal protein S30 fusion gene *fau*. N= 8. Data are expressed as the mean ± SEM. For each gene, asterisks indicate significant differences between SW and FW (*p < 0.05; **p < 0.01; ***p < 0.001). FW: fresh water; SW: seawater.

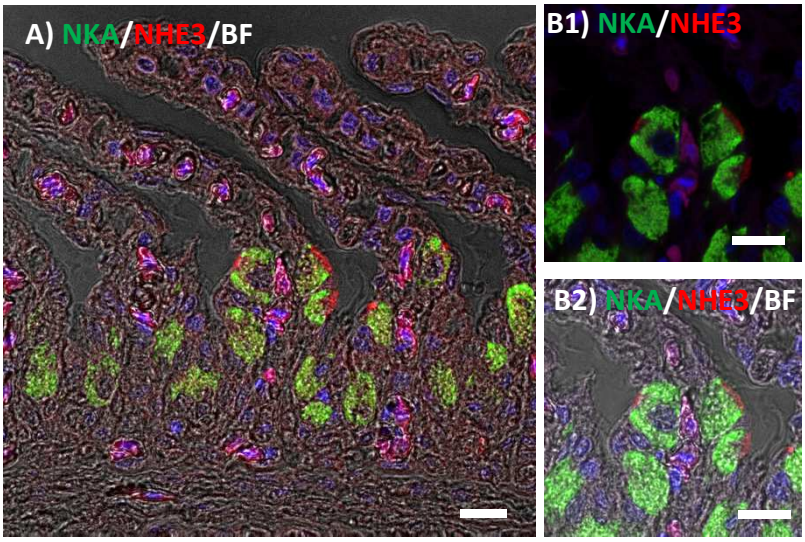

Fig. 5 Immunolocalization of Na^+/K^+-ATPase (NKA) (green) and Na^+/H^+-exchanger 3 (NHE3) (red) in gills of 2-weeks acclimated *D. labrax* to fresh water using low (A) and high (B1, B2) magnifications of the gill epithelium. Nuclei were counterstained with DAPI (blue). Note that NHE-expressing ionocytes are located on lamellae. BF: bright field. Scale : 10 µm.

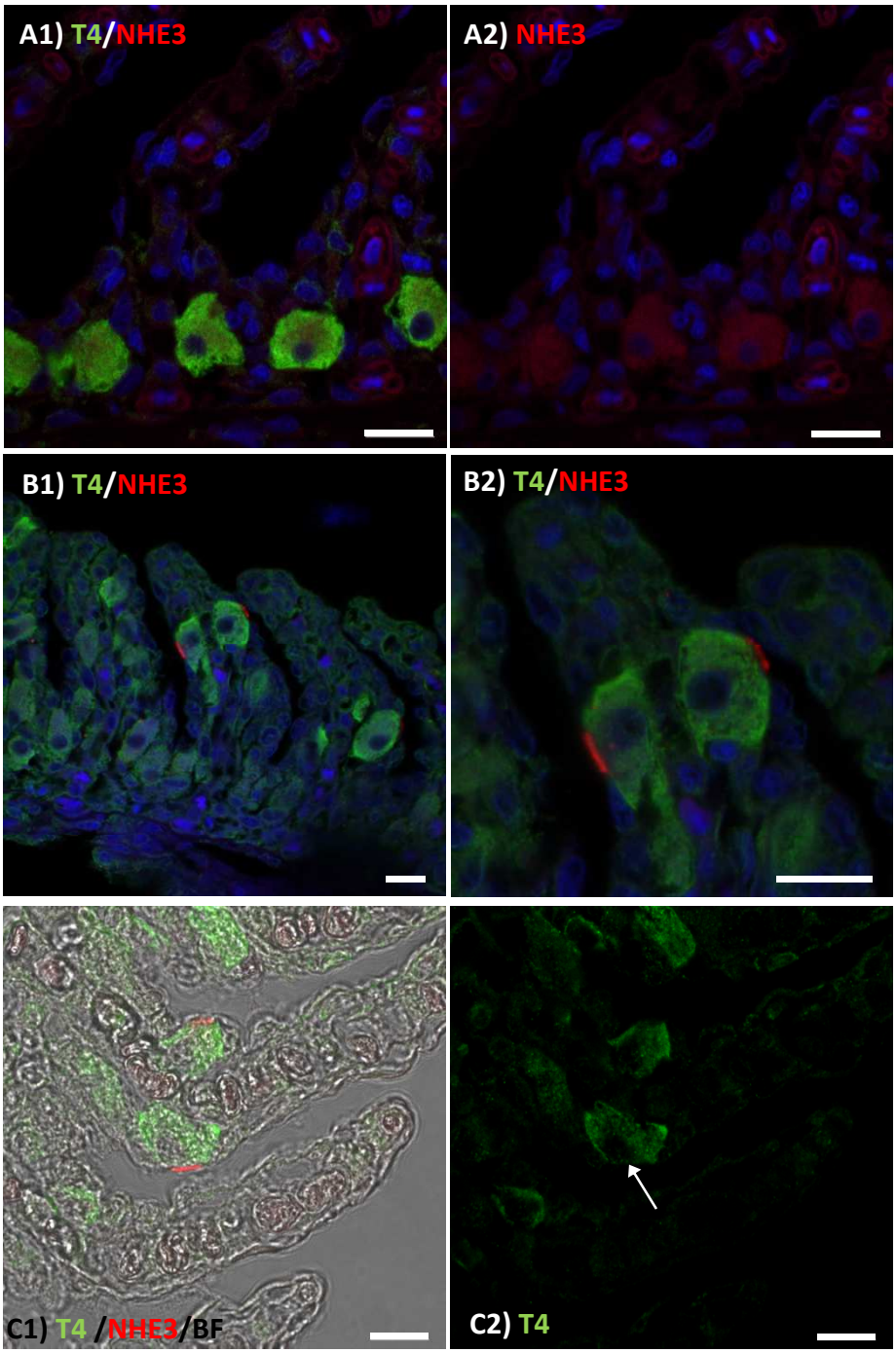

Fig. 6 Immunolocalization of NKCC1/NCC (T4) (green) and Na^+/H^+-exchanger 3 (NHE3) (red) in gills of seawater (A1, A2) and freshwater (2 weeks) acclimated *D. labrax* (B1, B2, C1, C2). Nuclei were counterstained with Dapi (blue, A1, A2, B1, B2). C2) The arrow indicates the absence of apical T4 staining in NHE3-type cells. B1), C1) Note that NHE3-expressing cells show strong basolateral T4 staining. BF: bright field. Scale : 10 µm.

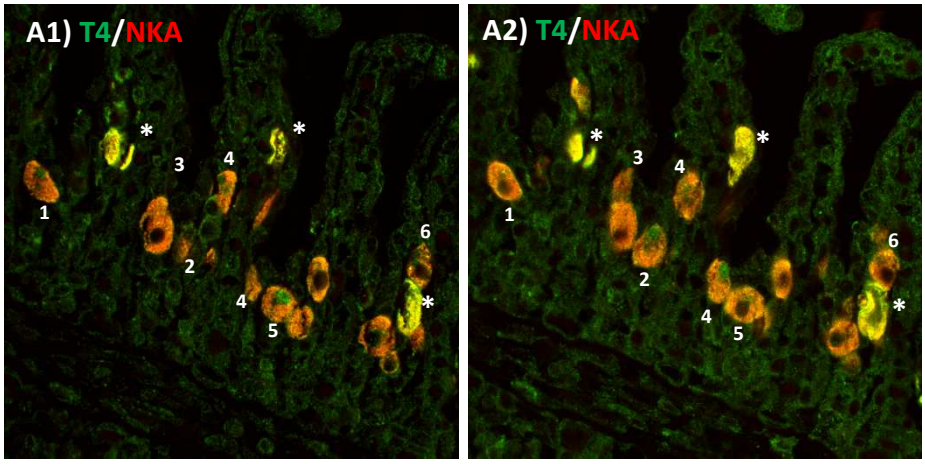

Fig. 7 Immunolocalization of NKCC1/NCC (T4) (green) and Na^+/K^+-ATPase (NKA) (red) in gills of 2-weeks acclimated *D. labrax* to fresh water. At least two ionocyte subtypes with apical (numbered) and basolateral (*) T4 staining are shown. A1, A2 images have been taken from a z-stack in order to identify NCC-type cells along the filament. Apical immunolabelling of T4 (numbered) is more or less visible across z-stack levels. Scale : 10 µm.

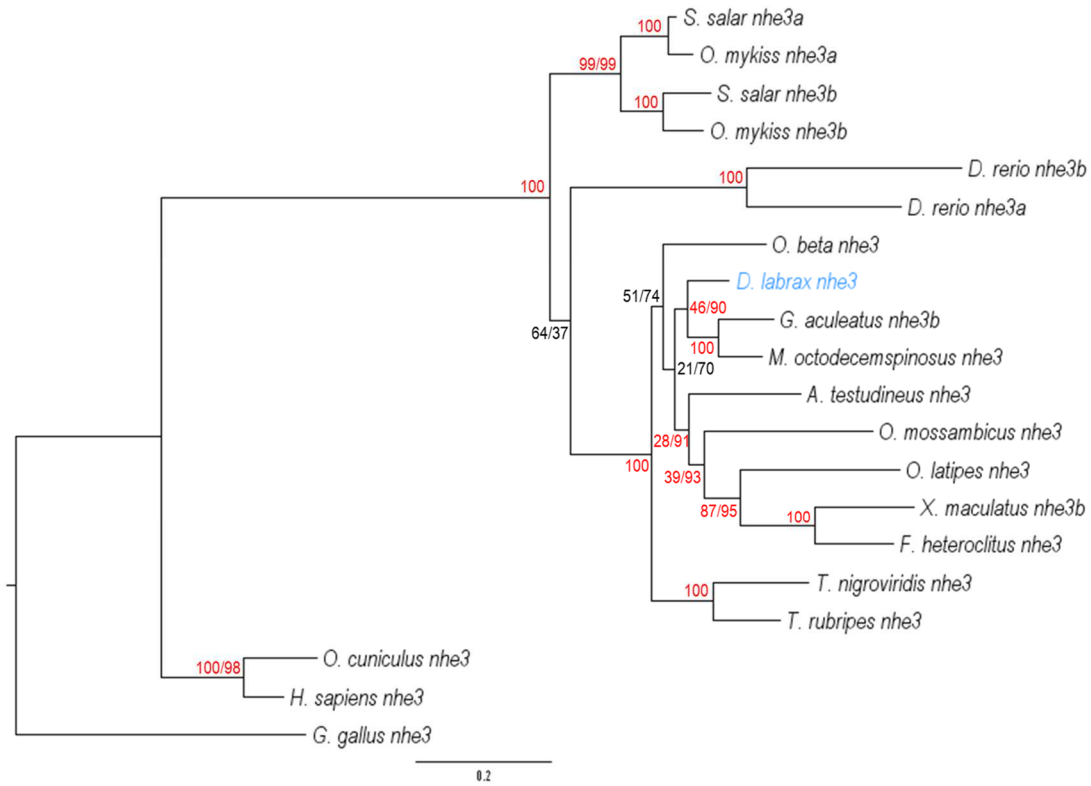

571

572

573 Fig. S1 Phylogenetic tree of *nhe3* (*scl9a3*). Phylogram of maximum likelihood relationships between
574 *nhe3*, *nhe3a* and *nhe3c* nucleotides sequences of representative acanthomorph and salmonid species.
575 Branch lengths represent degree of divergence, with the scale bar indicating the distance representing
576 0.2 substitutions per position. Bootstrap values (in %), and SH-like aLRT values are indicated for each
577 node if different (in red color if confident).

578

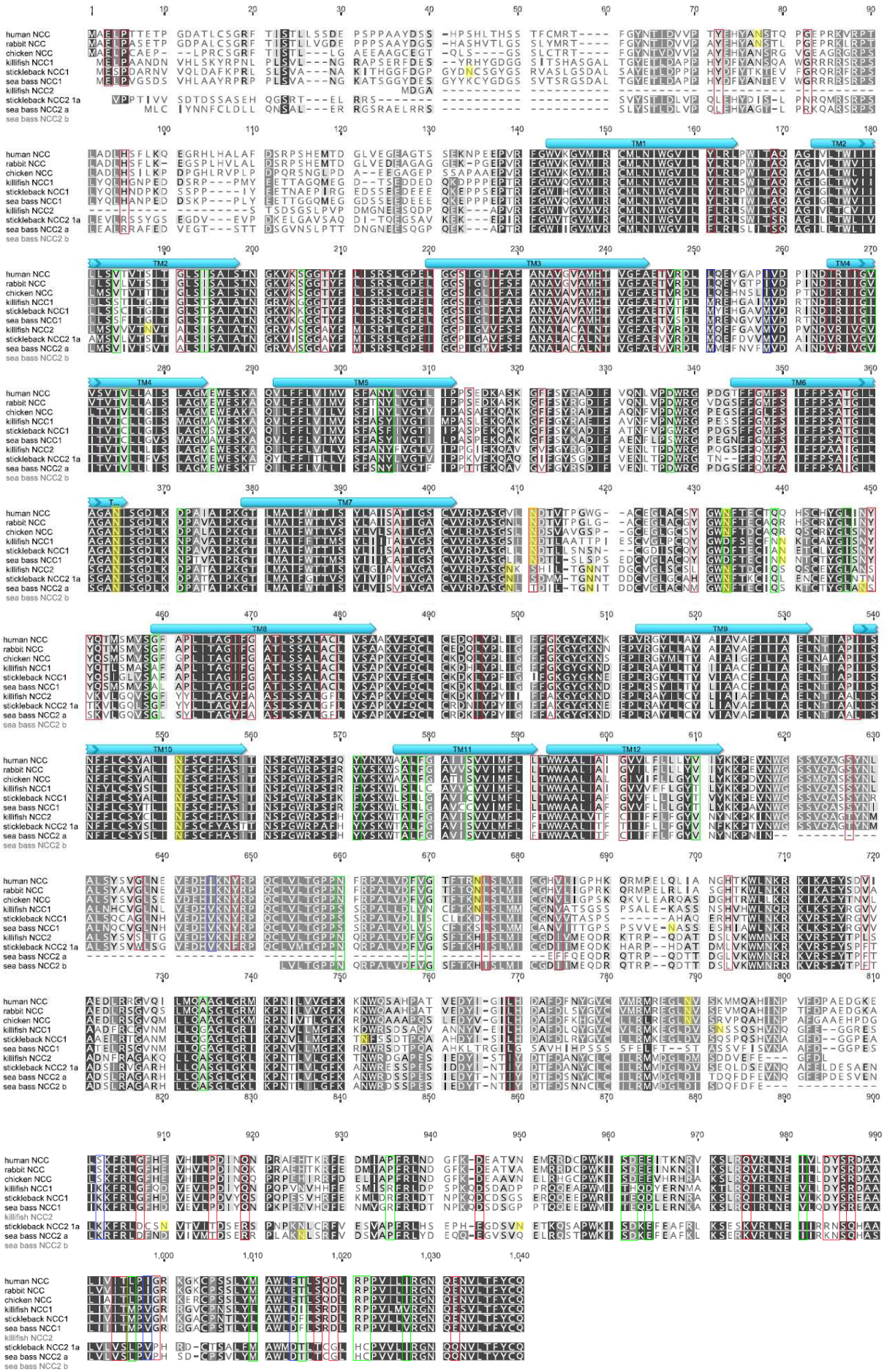
human NCC
rabbit NCC
chicken NCC
killifish NCC1
stickleback NCC1
sea bass NCC1
killifish NCC2
stickleback NCC2 1a
sea bass NCC2 a
sea bass NCC2 b
TM1
TM2
TM3
TM4
TM5
TM6
TM7
TM8
TM9
TM10
TM11
TM12

582 Fig. S2 Alignment analysis of amino acid sequences of the mammalian and teleostean NCCs including
583 *D. labrax*. The twelve predicted transmembrane regions (TM1–TM12) are indicated as blue arrows
584 above the human NCC sequence. Potential N-glycosylation sites are highlighted in yellow. Red and
585 green boxes respectively indicate conserved amino acids between mammalian NCC sequences and
586 fish NCC1 or NCC2 sequences. Blue boxes indicated conserved amino acids among NCC sequences
587 of fish.

588

589 Table 1: *nhe2 (slc9a2)* nucleotide sequences used in phylogenetic analyses
590
591
592

Nucleotide sequence ID	Fish species and gene
EF591983	*Danio rerio nhe2*
DLAgn_00111870	*Dicentrarchus labrax nhe2a*
DLAgn_00052750	*Dicentrarchus labrax nhe2b*
DLAgn_00136900	*Dicentrarchus labrax nhe2c*
AY818824	*Fundulus heteroclitus nhe2a*
EU886295	*Fundulus heteroclitus nhe2b*
NM_001285935	*Gallus gallus nhe2*
ENSGACT00000024567	*Gasterosteus aculeatus nhe2a*
ENSGACT00000003889.1	*Gasterosteus aculeatus nhe2b*
ENSGACT00000019807	*Gasterosteus aculeatus nhe2c*
NM_003048	*Homo sapiens nhe2*
AF159879	*Myoxocephalus octodecemspinosus nhe2b*
JN252127.1	*Myoxocephalus octodecemspinosus nhe2c*
NM_001130994	*Oncorhynchus mykiss nhe2*
HM134919	*Opsanus beta nhe2*
ENSONIT00000017898.1	*Oreochromis mossambicus nhe2*
XM_008253183	*Oryctolagus cuniculus nhe2*
ENSORLT00000015519.1	*Oryzia latipes nhe2*
XM_014174391	*Salmo salar nhe2*
XM_011610435	*Takifugu rubripes nhe2a*
XM_011608343	*Takifugu rubripes nhe2b*
ENSTNIT00000017095.1	*Tetraodon nigroviridis nhe2*
ENSXMAT00000011607.1	*Xiphophorus maculatus nhe2*

593
594
595
596
597
598
599
600

601 Table 2: *ncc1* (*slc12a3*) and *ncc2* (*slc12a10*) sequences used in phylogenetic analyses and sequences
602 analysis

Sequence ID	**Fish species and gene**
ENSDART00000010998.9	*Danio rerio slc12a3 / ncc1*
ENSDART00000023090.10	*Danio rerio slc12a10.1 / ncc2 1b*
ENSDART00000077616	*Danio rerio slc12a10.1 / ncc2 1a*
EF591989	*Danio rerio slc12a10.2 / ncc2 2*
ENSDART00000042955.7	*Danio rerio slc12a10.3 / ncc2 3a*
NM_001135131	*Danio rerio slc12a10.3 / ncc2 3b*
DLAgn_00172790	*Dicentrarchus labrax slc12a3 / ncc1*
DLAgn_00242670	*Dicentrarchus labrax slc12a10.2 / ncc2 b*
DLAgn_00038210	*Dicentrarchus labrax slc12a3-like / ncc2 a*
XM_021318983.1	*Fundulus heteroclitus slc12a3 / ncc1*
XM_021310632.1	*Fundulus heteroclitus slc12a3-like / ncc2*
ENSGALT00000004672.5	*Gallus gallus slc12a3 / ncc*
ENSGACT00000003177.1	*Gasterosteus aculeatus slc12a3 / ncc1*
ENSGACT00000025101.1	*Gasterosteus aculeatus slc10a10.1 / ncc2 1b*
ENSGACT00000025114.1	*Gasterosteus aculeatus slc12a10.1 / ncc2 1a*
NM_000339	*Homo sapiens slc12a3 / ncc*
XM_021570104	*Oncorhynchus mykiss slc12a3 / ncc1*
ENSONIT00000013415.1	*Oreochromis niloticus slc12a3 / ncc1*
ENSONIT00000009934.1	*Oreochromis niloticus slc12a10.1 / ncc2*
NM_001082649	*Oryctolagus cuniculus slc12a3 / ncc*
ENSORLT00000000509.1	*Oryzia latipes slc12a3 / ncc1*
ENSORLT00000023617.1	*Oryzia latipes slc12a10.1 / ncc2 1a*
ENSORLT00000025285.1	*Oryzia latipes slc12a10.1 / ncc2 1b*
XM_014149142	*Salmo salar slc12a3 / ncc1*
ENSTRUT00000023328.1	*Takifugu rubripes slc12a3 / ncc1*
ENSTNIT00000008076.1	*Tetraodon nigroviridis slc12a3 / ncc1*
ENSXMAT00000001059.1	*Xiphophorus maculatus slc12a10.1 / ncc2 1a*
ENSXMAT00000000940.1	*Xiphophorus maculatus slc12a10.1 / ncc2 1b*

603

Table 3: Primer sequences used for RT-PCR and qPCR in this study. ND: not determined. F: forward primer; R: reverse primer. Sequence ID indicate ID genome sequences from the sea bass genome or Genbank identification numbers when available.

Sequences ID	Target gene	Primer name	Sequence (from 5' to 3')	Amplicon Size	Efficiency
DLAgn_00057430	*slc9a1 / nhe1*	NHE1 F NHE1 R	TATCCCACAAGTCCCACACC CAAGAGGAAGCCAAGGGAGA	296	1.98
DLAgn_00204440	*scl9a1*-β / *nhe1*-β	NHE1-β F NHE1-β R	ACGGGGTTAATATGCGGCTT CAAGTTTCATGAGCAGGGCC	232	1.97
DLAgn_00052750	*slc9a2 / nhe2b*	NHE2b F NHE2b R	CTGTCAGATCGAGGCGTTTG TCAAACACACTCAGCACAGC	108	1.95
DLAgn_00136900	*scl9a2 / nhe2c*	NHE2c F NHE2c R	CGTTTCACCCACAATGTCCG GGGAATTGGCATTCTGGTGC	337	1.99
DLAgn_00204050	*slc9a3 / nhe3*	NHE3 F NHE3 R	GGATACCTCGCCTACCTGAC AAGAGGAGGGTGAGGAGGAT	251	1.98
DLAgn_00080120	*slc12a2 / nkcc1*	NKCC1 F NKCC1 R	TCAGCTCACAGTTCAAGGCC GCCGCTATGGACTCCACAA	102	2.08
DLAgn_00038210	*slc12a3-like / ncc2a*	NCC2a F NCC2a R	ATGATGAGCCTCTTCGAGCC GCTGCTCTCATCACCTTCTGT	278	1.94
DLAgn_00076370	*atp6v1a / vha-a*	VHA-A F VHA-A R	GGCAGTCACATCACAGGAGG CCAGCTCCATCACCACATCG	154	1.98
DLAgn_00018050	*atp6v1b2 / vha-b*	VHA-B F VHA-B R	TTGCCATAGTCTTCGCAGCC CTTCTCGCACTGGTAGGCC	194	1.90
KP400258	*atp1a1.a / nka α1a*	NKA a1a F NKA a1a R	CCTCAGATGGCAAGGAGAAG CCCTGCTGAGATCGGTTCC	146	1.89
KP400259	*atp1a1.b / nka α1b*	NKA α1b F NKA α1b R	AGCAGGGCATGAAGAACAAG CCTGGGCTGCGTCTGAGG	204	1.99
DLAgn_00078080	*cac (cahz)*	CAC F CAC R	CAGGGACCAAGTATCCTGC CCCTCCACCTTGCTCCCT	227	2.01
DLAgn_00082210	*slc4a4a / nbc1*	NBC1 F NBC1 R	ACAGAGCACGGAACACACGG CGTCCACAGCCAGCAGTTCG	182	1.96
DLAgn_00222650	*rhbg*	RHBG F1 RHBG R1	CCTCATGGTGACCCGAATCC GCCTGCACTCTGTCCACATA	218	1.97
DLAgn_00166370	*rhcg1*	RHCG1 F1 RHCG1 R1	TCAGGGAATTGTGTGACCGC AGAATCAAGTCCACGCTGGG	118	2.01
DLAgn_00157760	*rhcg2*	RHCG2 F1 RHCG2R1	TGGCTACCTGTTTGTCACGC GGATGCTCGGCGGCTTTATA	105	1.99
FM004681	*fau*	FAU-F FAU-R	GACACCCAAGGTTGACAAGCAG GGCATTGAAGCACTTAGGAGTTG	150	2.07
AJ866727	*ef1α*	EF1-F EF1-R	GGCTGGTATCTCTAAGAACG CCTCCAGCATGTTGTCTCC	239	2.09
DLAgn_00049060	*asic4*	ASIC4F ASIC4R	CATCTTCGTCTCTGGTCGCC GCTCTGAATGAAGAGGCGAC	149	1.84
DLAgn_00111870	*slc9a2/nhe2a*	NHE2a F NHE2a R	CTAGAGCCCAGGTCATTGCC GGCGTGTCCACAATACAGGA	244	ND

611 Table S1: *nhe3 (slc9a3)* nucleotide sequences used in phylogenetic analyses. Letters in brackets
612 indicate predicted paralogs.

Nucleotide sequence ID	**Fish species and gene**
KU555941	*Anabas testudineus nhe3*
EF591984	*Danio rerio nhe3a*
EF591980	*Danio rerio nhe3b*
DLAgn_00204050	*Dicentrarchus labrax nhe3*
AY818825	*Fundulus heteroclitus nhe3*
XM_418895	*Gallus gallus nhe3*
ENSGACT00000003204.1	*Gasterosteus aculeatus nhe3b*
NM_004174	*Homo sapiens nhe3*
EU909191	*Myoxocephalus octodecemspinosus nhe3*
NM_001130995	*Oncorhynchus mykiss nhe3a*
NM_001160482	*Oncorhynchus mykiss nhe3b*
HM134920	*Opsanus beta nhe3*
AB326212	*Oreochromis mossambicus nhe3*
NM_001082697	*Oryctolagus cuniculus nhe3*
XM_020707274	*Oryzia latipes nhe3*
XM_014166803	*Salmo salar nhe3(a)*
XM_014177059	*Salmo salar nhe3(b)*
XM_011609332	*Takifugu rubripes nhe3*
ENSTNIT00000005337.1	*Tetraodon nigroviridis nhe3*
ENSXMAT00000007256.1	*Xiphophorus maculatus nhe3b*

613

References

Blondeau-Bidet, E., Bossus, M., Maugars, G., Farcy, E., Lignot, J.-H., Lorin-Nebel, C., 2016. Molecular characterization and expression of Na^+/K^+-ATPase α1 isoforms in the European sea-bass *Dicentrarchus labra*x osmoregulatory tissues following salinity transfer. Fish Physiol. Biochem. 42, 1647-1664.

Bodinier, C., Lorin-Nebel, C., Charmantier, G., Boulo, V., 2009. Influence of salinity on the localization and expression of the CFTR chloride channel in the ionocytes of juvenile *Dicentrarchus labrax* exposed to seawater and freshwater. Comp. Biochem. Physiol. 153 345-351.

Bollinger, R.J., Madsen, S.S., Bossus, M.C., Tipsmark, C.K., 2016. Does Japanese medaka (*Oryzias latipes*) exhibit a gill Na^+/K^+-ATPase isoform switch during salinity change ? J. Comp. Physiol. B 186, 485-501.

Bossus, M., Charmantier, G., Blondeau-Bidet, E., Valletta, B., Boulo, V., Lorin-Nebel, C., 2013 The ClC-3 chloride channel and osmoregulation in the European Sea Bass, *Dicentrarchus labrax*. J. Comp. Physiol. B. 183, 641-662.

Breves, J.P., Seale, A.P., Moorman, B.P., Lerner, D.T., Moriyama, S., Hopkins, K.D., Grau, E.G., 2014. Pituitary control of branchial NCC, NKCC and Na^+, K^+-ATPase alpha-subunit gene expression in Nile tilapia, *Oreochromis niloticus*. J. Comp. Physiol. B 184, 513-523.

Chen, X.L., Zhang, B., Chng, Y.R., Ong, J.L.Y., Chew, S.F., Wong, W.P., Lam, S.H., Ip, Y.K., 2017. Na^+/H^+ exchanger 3 is expressed in two distinct types of ionocyte, and probably augments ammonia excretion in one of them, in the gills of the climbing perch exposed to seawater. Frontiers Physiol. 8, 880. doi: 10.3389/fphys.2017.00880.

Christensen, A.K., Hiroi, J., Schultz, E.T., McCormick, S.D., 2012. Branchial ionocyte organization and ion-transport protein expression in juvenile alewives acclimated to freshwater or seawater. J. Exp. Biol. 215, 642-652.

Claiborne, J.B., Blackston, C.R., Choe, K.P., Dawson, D.C., Harris, S.P., Mackenzie, L.A., Morrison-Shetlar, A.I., 1999. A mechanism for branchial acid excretion in marine fish: identification of multiple Na^+/H^+ antiporter (NHE) isoforms in gills of two seawater teleosts. J. Exp. Biol. 202, 315-324.

Cooper, C.A., Wilson, J.M., Wright, P.A., 2013. Marine, freshwater and aerially acclimated mangrove rivulus (*Kryptolebias marmoratus*) use different strategies for cutaneous ammonia excretion. Amer. J. Physiol. Regulat. Integr. Comp. Physiol. 304, R599-R612.

Dymowska, A.K., Boyle, D., Schultz, A.G., Goss, G.G., 2015. The role of acid-sensing ion channels in epithelial Na^+ uptake in adult zebrafish (*Danio rerio*). J. Exp. Biol. 218, 1244-1251.

Dymowska, A.K., Hwang, P.P., Goss, G.G., 2012. Structure and function of ionocytes in the freshwater fish gill. Respir. Physiol. Neurobiol. 184, 282-292.

Dymowska, A.K., Schultz, A.G., Blair, S.D., Chamot, D., Goss, G.G., 2014. Acid-sensing ion channels are involved in epithelial Na^+ uptake in the rainbow trout *Oncorhynchus mykiss*. Amer. J. Physiol. Cell Physiol. 307, C255-265.

Edgar, R.C., 2004. MUSCLE: multiple sequence alignment with high accuracy and high throughput. Nucleic Acids Res. 32, 1792-1797.

Edwards, S.L., Wall, B.P., Morrison-Shetlar, A., Sligh, S., Weakley, J.C., Claiborne, J.B., 2005. The effect of environmental hypercapnia and salinity on the expression of NHE-like isoforms in the gills of a euryhaline fish (*Fundulus heteroclitus*). J. Exp. Zool. A 303, 464-475.

Edwards, S.L., Weakley, J.C., Diamanduros, A.W., Claiborne, J.B., 2010. Molecular identification of Na^+-H^+ exchanger isoforms (NHE2) in the gills of the euryhaline teleost *Fundulus heteroclitus*. J. Fish Biol. 76, 415-426.

Esbaugh, A.J., Grosell, M., 2014. Esophageal desalination is mediated by Na(+), H(+) exchanger-2 in the gulf toadfish (*Opsanus beta*). Comp. Biochem. Physiol. A, Mol. Integr. Physiol. 171, 57-63.

Esbaugh, A.J., Perry, S.F., Bayaa, M., Georgalis, T., Nickerson, J., Tufts, B.L., Gilmour, K.M., 2005. Cytoplasmic carbonic anhydrase isozymes in rainbow trout *Oncorhynchus mykiss* : comparative physiology and molecular evolution. J. Exp. Biol. 208, 1951-1961.

Gamba, G., Saltzberg, S. N., Lombardi, M., Miyanoshita, A., Lytton, J., Hediger, M. A., ... , Hebert, S. C. , 1993. Primary structure and functional expression of a cDNA encoding the thiazide-sensitive, electroneutral sodium-chloride cotransporter. PNAS, 90, 2749-2753.

Genz, J., Esbaugh, A.J., Grosell, M., 2011. Intestinal transport following transfer to increased salinity in an anadromous fish *(Oncorhynchus mykiss*). Comp. Biochem. Physiol. A: Mol. Integ. Physiol. 159, 150-158.

Gilmour, K.M., 2012. New insights into the many functions of carbonic anhydrase in fish gills. Resp. Physiol. Neurobiol. 184, 223-230.

Glasauer, S.M., Neuhauss, S.C., 2014. Whole-genome duplication in teleost fishes and its evolutionary consequences. Mol. Genet. Genomics 289, 1045-1060.

Guh, Y.-J., Hwang, P.-P., 2017. Insights into molecular and cellular mechanisms of hormonal actions on fish ion regulation derived from the zebrafish model. Gen. Comp. Endocrinol. 251, 12-20.

Guindon, S., Gascuel, O., 2003. A simple, fast, and accurate algorithm to estimate large phylogenies by maximum likelihood. Systematic Biol. 52, 696-704.

Hiroi, J., McCormick, S.D., 2012. New insights into gill ionocyte and ion transporter function in euryhaline and diadromous fish. Respir. Physiol. Neurobiol. 184, 257-268.

Hiroi, J., Yasumasu, S., McCormick, S., Hwang, P.-P., Kaneko, T., 2008. Evidence for an apical Na-Cl cotransporter involved in ion uptake in a teleost fish. J. Exp. Biol. 211, 2584-2599.

Hsu, H.-H., Lin, L.-Y., Tseng, Y.-C., Horng, J.-L., Hwang, P.-P., 2014. A new model for fish ion regulation: identification of ionocytes in freshwater- and seawater-acclimated medaka (*Oryzias latipes*). Cell Tissue Res. 357, 225-243.

Hwang, P.-P., 2011. Mechanisms of ion transport in freshwater fishes. In: Farrell T., Stevens D, Cech J, Richards J (Eds.), Encyclopedia of Fish Physiology. San Diego: Elsevier Academia Press.

Hwang, P.P., 2009. Ion uptake and acid secretion in zebrafish (*Danio rerio*). J. Exp. Biol. 212, 1745-1752.

Hwang, P.P., Lee, T.H., Lin, L.Y., 2011. Ion regulation in fish gills: recent progress in the cellular and molecular mechanisms. Amer. J. Physiol. Regul. Integr. Comp. Physiol. 301, R28-R47.

Hwang, P.P., Lin, L.Y., 2013. Gill ionic transport, acid-base regulation, and nitrogen excretion, in: D.H. Evans, J.B. Clairborne (Eds.), The Physiology of Fishes, CRC Press, Boca Raton, FL, 205-233.

Inokuchi, M., Hiroi, J., Watanabe, S., Lee, K.M., Kaneko, T., 2008. Gene expression and morphological localization of NHE3, NCC and NKCC1a in branchial mitochondria-rich cells of Mozambique tilapia (*Oreochromis mossambicus*) acclimated to a wide range of salinities. Comp. Biochem. Physiol. A 151, 151-158.

Inokuchi, M., Nakamura, M., Miyanishi, H., Hiroi, J., Kaneko, T., 2017. Functional classification of gill ionocytes and spatiotemporal changes in their distribution after transfer from seawater to freshwater in Japanese seabass. J. Exp. Biol. 220, 4720-4732.

Ivanis, G., Esbaugh, A.J., Perry, S.F., 2008. Branchial expression and localization of SLC9A2 and SLC9A3 sodium/hydrogen exchangers and their possible role in acid-base regulation in freshwater rainbow trout (*Oncorhynchus mykiss)*. J. Exp. Biol. 211, 2467-2477.

Käll, L., Krogh, A., Sonnhammer, E.L. 2005. An HMM posterior decoder for sequence feature prediction that includes homology information. Bioinformatics, 21, i251-i257.

Katoh, F., Hyodo, S., Kaneko, T., 2003. Vacuolar-type proton pump in the basolateral plasma membrane energizes ion uptake in branchial mitochondria-rich cells of killifish *Fundulus heteroclitus*, adapted to a low ion environment. J. Exp. Biol. 206, 793-803.

Keane, T.M., Creevey, C.J., Pentony, M.M., Naughton, T.J., Mclnerney, J.O., 2006. Assessment of methods for amino acid matrix selection and their use on empirical data shows that ad hoc assumptions for choice of matrix are not justified. BMC Evol. Biol. 6, 29.

Kumai, Y., Perry, S.F., 2012. Mechanisms and regulation of Na^+ uptake by freshwater fish. Resp. Physiol. Neurobiol. 184, 249-256.

Laurent, P., Chevalier, C., Wood, C.M., 2006. Appearance of cuboidal cells in relation to salinity in gills of *Fundulus heteroclitus*, a species exhibiting branchial Na^+ but not Cl^- uptake in freshwater. Cell Tissue Res. 325, 481-492.

Lin, T.Y., Liao, B.K., Horng, J.L., Yan, J.J., Hsiao, C.D., Hwang, P.P., 2008. Carbonic anhydrase 2-like a and 15a are involved in acid-base regulation and Na^+ uptake in zebrafish H^+-ATPase-rich cells. Amer. J. Physiol. Cell Physiol. 294, C1250-1260.

Liu, S.T., Horng, J.L., Chen, P.Y., Hwang, P.P., Lin, L.Y., 2016. Salt secretion is linked to acid-base regulation of ionocytes in seawater-acclimated medaka: new insights into the salt-secreting mechanism. Sci. Reports 6, 31433.

Lorin-Nebel, C., Boulo, V., Bodinier, C., Charmantier, G., 2006. The $Na^+/K^+/2$ Cl^- cotransporter in the sea-bass *Dicentrarchus labrax* during ontogeny: Involvement in osmoregulation J. Exp. Biol. 209, 4908-4922.

Masroor, W., Farcy, E., Gros, R., Lorin-Nebel, C., 2018. Effect of combined stress (salinity and temperature) in European sea bass *Dicentrarchus labrax* osmoregulatory processes. Comp. Biochem. Physiol. A Mol. Integr. Physiol. 215, 45-54.

Meyer, A., Van de Peer, Y., 2005. From 2R to 3R: evidence for a fish-specific genome duplication (FSGD). BioEssays : news and reviews in molecular, cellular and developmental biology 27, 937-945.

Mitter, K., Kotoulas, G., Magoulas, A., Mulero, V., Sepulcre, P., Figueras, A., Novoa, B., Sarropoulou, E., 2009. Evaluation of candidate reference genes for QPCR during ontogenesis and of immune-relevant tissues of European sea bass (*Dicentrarchus labrax*). Comp. Biochem. Physiol. B 153, 340-347.

Nakada, T., Hoshijima, K., Esaki, M., Nagayoshi, S., Kawakami, K., Hirose, S., 2007. Localization of ammonia transporter Rhcg1 in mitochondrion-rich cells of yolk sac, gill, and kidney of zebrafish and its ionic strength-dependent expression. Amer. J. Physiol. Regul. Integr. Comp. Physiol. 293, R1743-1753.

Nebel, C., Romestand, B., Nègre-Sadargues, G., Grousset, E., Aujoulat, F., Bacal, J., Bonhomme, F., Charmantier, G., 2005. Differential freshwater adaptation in juvenile sea-bass *Dicentrarchus labrax* : Gill and urinary system involvement J. Exp. Biol. 208, 3859-3871.

Pfaffl, M. W., 2001. A new mathematical model for relative quantification in real-time RT–PCR. Nucleic Acids Res. 29, e45.

Posada, D., 2003. Using MODELTEST and PAUP* to select a model of nucleotide substitution. Curr. Protoc. Bioinformatics., 5-6. doi: 10.1002/0471250953.bi0605s00.

Seo, M., Mekuchi, M., Teranishi, K., Kaneko, T., 2013. Expression of ion transporters in gill mitochondrion-rich cells in Japanese eel acclimated to a wide range of environmental salinity. Comp. Biochem. Physiol. A Mol. Integr. Physiol. 166: 323-332.

Shih, T.-H., Horng, J.-L., Liu, S.-T., Hwang, P.-P., Lin, L.-Y., 2012. Rhcg1 and NHE3b are involved in ammonium-dependent sodium uptake by zebrafish larvae acclimated to low-sodium water. Amer. J. Physiol. 302, R84-R93.

Shih, T.H., Horng, J.L., Hwang, P.P., Lin, L.Y., 2008. Ammonia excretion by the skin of zebrafish (*Danio rerio*) larvae. Amer. J. Physiol. Cell Physiol. 295, C1625-1632.

Sinha, A.K., AbdElgawad, H., Zinta, G., Dasan, A.F., Rasoloniriana, R., Asard, H., Blust, R., De Boeck, G., 2015. Nutritional Status as the Key Modulator of Antioxidant Responses Induced by High Environmental Ammonia and Salinity Stress in European Sea Bass (*Dicentrarchus labrax*). PLoS One 10, e0135091.

Takei, Y., Hiroi, J., Takahashi, H., Sakamoto, T., 2014. Diverse mechanisms for body fluid regulation in teleost fishes. Amer. J. Physiol. Regul. Integr. Comp. Physiol. 307, R778-792.

Talavera, G., Castresana, J., 2007. Improvement of phylogenies after removing divergent and ambiguously aligned blocks from protein sequence alignments. Systematic Biology 56, 564-577.

Tavaré, S., 1986. Some probabilistic and statistical problems in the analysis of DNA sequences. Lect. Math. Life Sci. 17, 57–86.

Tine, M., Kuhl, H., Gagnaire, P.-A., Louro, B., Desmarais, E., Martins, R.S.T., Hecht, J., Knaust, F., Belkhir, K., Klages, S., Dieterich, R., Stueber, K., Piferrer, F., Guinand, B., Bierne, N., Volckaert, F.A.M., Bargelloni, L., Power, D.M., Bonhomme, F., Canario, A.V.M., Reinhardt, R., 2014. European sea bass genome and its variation provide insights into adaptation to euryhalinity and speciation. Nat. Commun. 5, 5770. doi: 10.1038/ncomms6770.

Tse, M., Levine, S., Yun, C., Brant, S., Counillon, L.T., Pouyssegur, J., Donowitz, M., 1993. Structure/function studies of the epithelial isoforms of the mammalian Na^+/H^+ exchanger gene family. J. Membr. Biol. 135, 93-108.

Wang, Y.F., Tseng, Y.C., Yan, J.J., Hiroi, J., Hwang, P.P., 2009. Role of SLC12A10.2, a Na-Cl cotransporter-like protein, in a Cl uptake mechanism in zebrafish (*Danio rerio*). Amer. J. Physiol. Regul. Integr. Comp. Physiol. 296, R1650-1660.

Watanabe, S., Niida, M., Maruyama, T., Kaneko, T., 2008. Na^+/H^+ exchanger isoform 3 expressed in apical membrane of gill mitochondrion-rich cells in Mozambique tilapia *Oreochromis mossambicus*. Fisheries Sci. 74, 813-821.

Weihrauch, D., Wilkie, M.P., Walsh, P.J., 2009. Ammonia and urea transporters in gills of fish and aquatic crustaceans. J. Exp. Biol. 212, 1716-1730.

Wright, P.A., Wood, C.M., 2009. A new paradigm for ammonia excretion in aquatic animals: role of Rhesus (Rh) glycoproteins. J. Exp. Biol. 212, 2303-2312.

Wright, P.A., Wood, C.M., Hiroi, J., Wilson, J.M., 2016. (Uncommon) mechanisms of branchial ammonia excretion in the common carp (*Cyprinus carpio*) in response to environmentally induced metabolic acidosis. Physiol. Biochem. Zool. 89, 26-40.

Wu, S.-C., Horng, J.-L., Liu, S.-T., Hwang, P.-P., Wen, Z.-H., Lin, C.-S., Lin, L.-Y., 2010. Ammonium-dependent sodium uptake in mitochondrion-rich cells of medaka (*Oryzias latipes*) larvae. Amer. J. Physiol. Cell Physiol. 298, C237-C250.

Yan, J.J., Chou, M.Y., Kaneko, T., Hwang, P.P., 2007. Gene expression of Na^+/H^+ exchanger in zebrafish H^+ -ATPase-rich cells during acclimation to low-Na^+ and acidic environments. Amer. J. Physiol. Cell Physiol 293.